FOREX Publication
Open Access | Rapid and quality publishing

International Journal of Electrical and Electronics Research (IJEER)
Research Article | Volume 13, Issue 4 | Pages 861-869 | e-ISSN: 2347-470X

Energy-Efficient Sub-Millisecond DWDM Backhaul for 6G Open RAN

Ali Abduljabbar Abdulsattar[1], Hussein Shakor Mogheer[2], Mohammad S. Al-Abadi[3], and Yassir AL-Karawi[4*]

[1]*Assistant Lecturer, Department of Communications Engineering, College of Engineering, University of Diyala, Baqubah, Iraq*
[2]*Lecturer, Department of Communications Engineering, College of Engineering, University of Diyala, Baqubah, Iraq*
[3]*Lecturer, Department of Communications Engineering, College of Engineering, University of Diyala, Baqubah, Iraq*
[4]*Assistant Professor, Department of Communications Engineering, College of Engineering, University of Diyala, Baqubah, Iraq*

***Correspondence:** *Yassir AL-Karawi*, Email: *yassir_al-karawi_eng@uodiyala.edu.iq*

ABSTRACT- Wavelength-aware and constraint-driven framework is presented for dense WDM optical backhaul in 6G Open RAN. The design jointly minimizes energy while enforcing explicit sub-millisecond delay bounds under non-stationary traffic and integrates cleanly with near-RT RIC control. A three-stage controller computes a feasible allocation through projected primal–dual updates then perform energy-aware wavelength pruning and finally executes latency-responsive reconfiguration on incipient violations. Evaluation across diverse topologies and bursty as well as diurnal loads shows up to 32% lower optical power than static provisioning with delays concentrated in 0.7–0.8*ms* and low control overhead. Comparative experiments against greedy heuristics and a lightweight actor–critic baseline indicate superior energy–latency trade-offs and fewer violations above one millisecond. A complexity analysis shows per-interval updates scale as $O(|\mathcal{E}||\mathcal{W}|)$ and fit within near-real-time control cycles which supports practical deployment feasibility on commodity RIC servers. The approach operationalizes elastic optical networking as a first-class dimension for ORAN backhaul and offers a deployable path to greener and delay-bounded transport for 6G services.

Keywords: 6G Optical Backhaul, DWDM, O-RAN, Lagrangian Optimization, Energy–Latency Optimization, near-RT RIC.

ARTICLE INFORMATION

Author(s): Ali Abduljabbar Abdulsattar, Hussein Shakor Mogheer, Mohammad S. Al-Abadi, Yassir AL-Karawi;

Received: 13/06/2025; **Accepted:** 03/11/2025; **Published:** 25/12/2025;
E- ISSN: 2347-470X;
Paper Id: IJEER 1306-09;
Citation: 10.37391/ijeer.1304--
Webpage-link:
https://ijeer.forexjournal.co.in/archive/volume-13/ijeer-1304--.html

Publisher's Note: FOREX Publication stays neutral with regard to jurisdictional claims in Published maps and institutional affiliations.

1. INTRODUCTION

6G is poised to usher in a new era of mobile networking with extreme data rates, sub-millisecond latency, high energy efficiency, and mission-critical reliability [1], [2], [3], [4]. In contrast to earlier generations focused on broadband capacity, 6G targets immersive and interactive services such as holographic telepresence, XR, autonomous robotics, and pervasive AI [5], [6]. Meeting these targets requires rethinking the transport layer as well as the radio interface.

Open RAN decouples radio units (RUs), distributed units (DUs), and centralized units (CUs) *via* standardized interfaces and cloud-native orchestration [7], [8]. Static wavelength provisioning in disaggregated Open RAN has been identified as a major contributor to energy waste [9], [10]. Optical fibre with DWDM and elastic spectrum offers ultrahigh capacity and microsecond propagation, enabling adaptive wavelength management under time-varying loads [11], [12], [13], [14], [15], [16]. Despite this potential, current deployments often lack real-time, traffic-aware, and energy-aware control across ROADMs and WSSs, which leads to underutilization and latency risk [17], [18], [19], [20].

Related efforts in SDN control and quantum-aware resource models indicate pathways for faster adaptation and fewer service-level violations. Ongoing ITU, ETSI, and IEEE activities further motivate transport designs that are latency-compliant and energy-efficient for 6G [21], [22].

1.1. Contributions

(i) An Open RAN backhaul architecture that integrates DWDM-based dynamic wavelength management for real-time adaptation to spatio-temporal traffic and energy limits. *(ii)* A latency-constrained and energy-aware wavelength-assignment formulation using a Lagrangian framework that captures traffic dynamics and physical constraints. *(iii)* A three-stage algorithm combining projected primal–dual allocation, energy-aware refinement, and delay-responsive reconfiguration. *(iv)* An evaluation showing up to 32% energy reduction with sub-millisecond end-to-end delay across multiple topologies and traffic profiles.

1.2. Organization

Section 2 surveys related optical transport for 5G/6G and links to Open RAN. *Section 3* outlines the architecture. *Section 4* presents the optimization model. *Section 5* details the algorithm. *Section 6* reports results. *Section 7* concludes.

FOREX Publication
Open Access | Rapid and quality publishing
International Journal of Electrical and Electronics Research (IJEER)
Research Article | Volume 13, Issue 4 | Pages 861-869 | e-ISSN: 2347-470X

2. RELATED WORK

Optical fibre has long underpinned high throughput and low latency targets in mobile systems [16], [17]. Early efforts focused on fixed capacity backhaul in legacy architectures and highlighted the advantage of fibre over wireless transport. As networks shifted toward modular and disaggregated designs static deployment models became increasingly inadequate.

The emergence of Cloud RAN and Open RAN introduced physical separation of RUs DUs and CUs with new transport demands [12], [13]. Foundational studies such as Checko et al. analysed transport implications and stressed the need for high capacity and low jitter fronthaul. Many Open RAN studies still treat transport as a passive pipe rather than an intelligent and reconfigurable layer [15].

Recent work on elastic optical networking and WDM demonstrated dynamic spectrum agility and flexible grid models [19], [20]. Translation of these principles to RAN backhaul remains limited. Many RAN optical solutions continue to rely on static wavelength assignment or predefined configurations that do not align with highly dynamic 6G traffic.

Energy efficiency for optical backhaul has received sustained attention. Surveys and models on power aware routing and ROADM based meshes established core power and switching delay models [21]. Service oriented delay guarantees are often absent despite their importance for tactile and immersive traffic.

Latency sensitive optimization has also advanced. Wang and Li proposed delay aware topology design for 6G oriented systems [4]. Most approaches target core or metro scale scenarios with fewer constraints from short hop and edge proximal RAN transport. Emerging directions include reconfigurable meta surfaces and neural optics for short reach photonics [25], [26], [10] and energy aware links with OAM multiplexing [27]. A joint formulation that aligns wavelength assignment with explicit latency bounds remains limited in prior art.

SDN and control plane intelligence for optical access suggest fine grained programmability [28], [29]. Practical real time optimization strategies that scale to Open RAN backhaul are still scarce. Traffic aware resource allocation in software centric wireless systems exists [3], [30] yet it often abstracts optical layer constraints.

Standardization efforts by ITU ETSI and IEEE emphasize flexible energy aware and latency compliant transport [31]. Prescriptive models for Open RAN optical backhaul that combine elastic spectrum control with near real time delay guarantees remain under specified.

Positioning relative to AI and ML Studies based on greedy heuristics and deep reinforcement learning including DQN and PPO explore dynamic allocation. Reported methods often lack explicit feasibility guarantees for delay and can incur non trivial training cost and control overhead. Constraint driven formulations with Lagrangian control provide bounded per interval complexity and clean integration with near RT RIC which motivates benchmarking against greedy and actor critic baselines.

TABLE 1. Condensed landscape of related work and the gap

Ref.	Focus	Research Gap
[23]	EON for 5G	No Open RAN link and no energy–delay coupling
[24]	SDN optical control	Limited DWDM reconfigurability for modular RAN
[21]	Energy aware routing	Lacks explicit latency feasibility
[22]	Delay bounded paths	Omits power coupling and spectrum dynamics
[5]	Transponder planning	Static without adaptation to traffic shifts
[7]	Wireless SDN	Abstracts optical layer and lacks DWDM granularity
This Paper	6G Open RAN backhaul	Unified DWDM plus latency control with real-time reconfigurability

3. SYSTEM ARCHITECTURE

A wavelength-aware, multi-stage optimization architecture is adopted for energy-efficient and low-latency optical backhaul in 6G Open RAN. The transport layer employs dense WDM (DWDM) between distributed and centralized domains, with ROADMs and WSS elements providing per-wavelength agility. Radio units connect to distributed units through fronthaul fibre links that must satisfy stringent delay and synchronization requirements due to lower layer processing.

A single near-RT RIC instance, co-located with the CU or logically centralized, orchestrates dynamic wavelength assignment using a three-stage control loop;

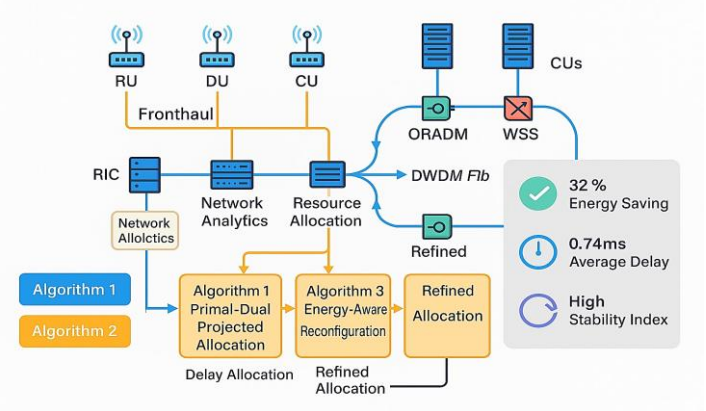

Figure 1. Multi-stage wavelength-aware optimization framework for energy-efficient 6G Open RAN optical backhaul

1. Projected primal–dual allocation that enforces bandwidth and sub-ms delay feasibility within the available power envelope.
2. Energy-aware refinement that prunes low-utility wavelengths while rechecking feasibility constraints.
3. Latency-responsive reconfiguration that reroutes flows upon incipient violations to low-queue and low-dispersion paths with bounded reconfiguration overhead.

FOREX Publication
Open Access | Rapid and quality publishing
International Journal of Electrical and Electronics Research (IJEER)
Research Article | Volume 13, Issue 4 | Pages 861-869 | e-ISSN: 2347-470X

Control and telemetry integrate with O-RAN functions. E2 carries control actions for wavelength (de)activation and path updates. A1 conveys policies and energy–latency weights for runtime tuning. O1 streams optical and queue measurements that feed allocation, refinement, and reconfiguration triggers.

DWDM links adapt channel width, modulation order, and transponder power according to traffic conditions and service level objectives. Traffic forecasting and QoS indicators enable pre-emptive mitigation of XR and tactile bursts through proactive wavelength reassignment. Runtime coordination between the optical layer and RAN scheduling supports spatial and temporal load variability with bounded jitter.

The modular form factor supports concurrent services using wavelength slicing and SLA-driven mapping over shared fibre infrastructure. This design preserves scalability for Open RAN deployments while meeting energy and latency targets characteristic of 6G systems.

4. MATHEMATICAL OPTIMIZATION FRAMEWORK

This section formalizes a wavelength–aware optimization framework that balances energy consumption and latency on DWDM backhaul links in Open RAN environments under spatio–temporal traffic variability. The goal is a constrained scheme that dynamically assigns wavelengths while meeting per–flow delay targets and per–link capacity limits.

4.1. System Model and Layered Representation

The optical transport is modelled as a directed fibre graph $\mathcal{G} = (\mathcal{V}, \mathcal{E})$ whose nodes $\mathcal{V}$ represent RUs, DUs, and CUs, and whose directed edges $\mathcal{E}$ represent fibre spans. Each link $(i,j) \in \mathcal{E}$ is characterized by length l_{ij}, attenuation α_{ij}, and chromatic dispersion D_{ij} [1], [2]. The propagation speed in fibre is denoted by v.

At the spectral layer, each span supports a configurable set of wavelengths compliant with ITU–T G.694.1 [5]. Each wavelength has bandwidth η_w, time–varying modulation order $M_w(t)$, and an efficiency factor γ_w that accounts for FEC and guard bands [6]. The achievable bitrate on wavelength w at time t is:

At the spectral layer, each span supports a configurable set of wavelengths compliant with ITU–T G.694.1 [5]. Each wavelength has bandwidth η_w, time–varying modulation order $M_w(t)$, and an efficiency factor γ_w that accounts for FEC and guard bands [6]. The achievable bitrate on wavelength w at time t is:

$$R_\omega(t) = \eta_\omega . \log_2(M_\omega(t) . \gamma_\omega \quad (1)$$

At the traffic layer, a time–varying demand $\lambda_f(t)$is associated with each flow $f \in \mathcal{F}$. Burstiness is captured through a BMAP–style component $\zeta_f(t)$. Power per active wavelength on link (i,j) is:

$$P_{ij}^{(\omega)}(t) = P_{tx}^{(\omega)} + P_{rx}^{(\omega)} + P_{amp}^{(ij,\omega)} \quad (2)$$

Which aggregates transmitter, receiver, and amplification terms [7], [8].

End–to–end latency for flow f traversing path $\mathcal{P}_f$ combines propagation, queueing, and reconfiguration delays:

$$D_f(t) = \sum_{(i,j)\in\mathcal{P}_f} \left(\frac{l_{ij}}{v} + q_{ij}(t) + \delta_{ij}^{(w)}(t)\right), \quad (3)$$

Where $q_{ij}(t)$denotes queueing delay and $\delta_{ij}^{(\omega)}(t)$ captures configuration time of wavelength w on span (i,j) [9], [11].

TABLE 2. Key notation used in the optimization framework

Symbol	Meaning
$\mathcal{G} = (\mathcal{V}, \mathcal{E})$	Directed optical graph
$l_{ij}, \alpha_{ij}, D_{ij}$	Span length, attenuation, dispersion on (i,j)
$w \in \mathcal{W}$, η_w, $M_w(t)$, γ_w	Wavelength, bandwidth, modulation, efficiency
$R_w(t)$	Bitrate on wavelength w at time t
$\lambda_f(t), \zeta_f(t)$	Flow demand and burstiness
$P_{ij}^{(\omega)}(t)$	Power of wavelength w on (i,j)
$q_{ij}(t), \delta_{ij}^{(\omega)}(t)$	Queueing and reconfiguration delays
$x_{ij}^{(w)}(t) \in \{0,1\}$	Assignment of wavelength w on (i,j)
$B_f(t)$	Aggregate bandwidth allocated to flow f
$C_{ij}^{(w)}$	Capacity of (i,j) on wavelength w
$D_f(t), D_f^{max}$	End–to–end delay and flow deadline
μ_f, ν_f	Dual variables for delay and demand constraints

4.2. Decision Variables and Constraints

Binary variables $x_{ij}^{(w)}(t)$ indicate activation of wavelength w on span (i,j) at time t:

$$x_{ij}^{(w)}(t) = \begin{cases} 1, & \text{if } w \text{ is assigned on } (i,j) \text{ at } t, \\ 0, & \text{otherwise.} \end{cases} \quad (4)$$

The aggregate bandwidth delivered to flow f satisfies

$$B_f(t) = \sum_{(i,j)\in\mathcal{P}_f} \sum_{w\in\mathcal{W}} x_{ij}^{(w)}(t)\, R_w(t), \quad (5)$$

and must meet its instantaneous demand

$$B_f(t) \geq \lambda_f(t), \quad \forall f \in \mathcal{F}, \quad (6)$$

URLLC–style latency requirements are enforced by

$$D_f(t) \leq D_f^{\max}, \quad \forall f \in \mathcal{F}, \quad (7)$$

Per–wavelength capacity on each span is respected through

$$\sum_{f\in\mathcal{F}} x_{ij}^{(w)}(t)\, R_w(t) \leq C_{ij}^{(w)}, \quad \forall (i,j),\ w, \quad (8)$$

4.3. Objective and Lagrangian Dual

The primary objective minimizes instantaneous optical power subject to feasibility:

$$\min_{x_{ij}^{(w)}(t)} \sum_{(i,j)\in\mathcal{E}} \sum_{w\in\mathcal{W}} x_{ij}^{(w)}(t)\, P_{ij}^{(w)}(t), \quad (9)$$

Coupling across delay and demand constraints yields a mixed–integer nonlinear program.

A Lagrangian relaxation introduces dual variables μ_f and ν_f for delay and demand constraints, and is solved via projected subgradient updates. The Lagrangian is:

FOREX Publication
Open Access | Rapid and quality publishing
International Journal of Electrical and Electronics Research (IJEER)
Research Article | Volume 13, Issue 4 | Pages 861-869 | e-ISSN: 2347-470X

$$\mathcal{L}(x,\mu,\nu) = \sum_{(i,j)} \sum_{w} x_{ij}^{(w)}(t)\, P_{ij}^{(w)}(t), + \sum_{f\in\mathcal{F}} \mu_f \left(D_f(t) - {D_f}^{max}\right), + \sum_{f\in\mathcal{F}} \nu_f \left(\lambda_f(t) + B_f(t)\right), \quad (10)$$

with dual

$$\max_{\mu_f\geq 0,\ \nu_f\geq 0} \min_{x_{ij}^{(w)}(t)} \mathcal{L}(x,\mu,\nu), \quad (11)$$

4.4. Primal–Dual Iterations and Feasibility Projection

Primal variables evolve with a projected step

$$x_{ij}^{(w)}(t+1) = \Pi_x[x_{ij}^{(w)}(t) - \alpha_t \nabla_x \mathcal{L}], \quad (12)$$

while dual variables follow

$$\mu_f(t+1) = [\mu_f(t) + \alpha_t(D_f(t) - {D_f}^{max}]^+ \quad (13)$$

$$\nu_f(t+1) = [\nu_f(t) + \alpha_t(\lambda_f(t) - B_f(t)]^+ \quad (14)$$

With a diminishing step α_t for stability [14]. The projection $\Pi_{\mathcal{X}}$ uses a light–weight capacity trim and a min–delay repair to restore feasibility under *eq. (8), (6)*, and *(7)*.

4.5. Path and Scheduling Heuristics

An energy–aware path choice selects a candidate path with lowest optical power subject to the delay bound:

$$\mathcal{P}_f^* = \operatorname{argmin}_{\mathcal{P}_f^{\text{cand}}} P_{\mathcal{P}_f} \quad \text{s.t.} \quad D_f(\mathcal{P}_f) \leq D_f^{\max}. \quad (15)$$

A delay–aware priority score guides wavelength scheduling, with higher priority for flows exhibiting larger measured queueing and controlled by a decay factor [16]. These heuristics preserve feasibility while improving convergence speed.

4.6. Network Metrics and Multi–Objective View

A normalized power metric summarizes network footprint,

$$\bar{P}(t) = \frac{1}{|\mathcal{E}|}\sum_{(i,j)\in\mathcal{E}} \frac{P_{ij}(t)}{P_{\max}}, \quad (16)$$

And a latency index captures sustained proximity to the deadline,

$$\Phi_f = \frac{1}{T}\sum_{t=1}^{T} \frac{D_f(t)}{D_f^{\max}}, \quad (17)$$

A scalarized analysis combines a logarithmic delay utility with an energy–latency trade–off index to trace Pareto behaviour, with a bounded–variation condition.

$$|\delta_{ij}^{(w)}(t) - \delta_{ij}^{(w)}(t-1)| \leq \Delta_{\max} \quad (18)$$

to limit configuration churn.

4.7. Problem Statement

The overall objective minimizes the expected composite cost under the full constraint set, generating slot–wise decisions compatible with near–real–time execution on the RIC:

$$\min\ \mathbb{E}\left[\sum_f \text{ELTI}_f\right] \text{ s.t. (4)–(8), (12)–(18)} \quad (19)$$

The resulting solution integrates energy awareness, latency compliance, and limited reconfiguration overhead, which aligns with service targets in 6G Open RAN transport [31].

5. PROPOSED ALGORITHMIC FRAMEWORK

A tri–stage controller is adopted to realize dynamic DWDM wavelength management under energy and latency constraints while keeping near-real-time feasibility on the RIC. The three stages address distinct control intents: feasible allocation under load and delay, energy refinement via marginal utility, and fast reconfiguration upon incipient SLA risk. Figure 2 illustrates the data flow among the stages and the RIC interface.

5.1. Stage 1: Primal–Dual Projected Allocation

This stage computes an initial feasible assignment by minimizing the dualized objective subject to bandwidth and delay constraints. Inputs: current traffic snapshot $\lambda_f(t)$, queueing measurements$q_{ij}(t)$, link attributes and available wavelengths. Outputs: a feasible binary map $x_{ij}^{(w)}(t)$ and updated multipliers (μ_f, ν_f) that penalize delay and unmet demand. Intuition: larger μ_f pushes flows with rising latency toward faster paths or higher$R_w(t)$, whereas larger ν_f adds bandwidth where $\lambda_f(t)$ exceeds $B_f(t)$.

Algorithm 1. *Primal–Dual Projected Allocation with Feasibility Projection*

1. *Initialize multipliers μ_f, ν_f and a feasible $x_{ij}^{(w)}(t)$ from the previous slot*
2. ***for** each time slot t **do***
3. *Sense $\lambda_f(t)$ and $q_{ij}(t)$, on the **RIC** northbound interface*
4. *Compute tentative $x_{ij}^{(w)}(t)$ by minimizing $\mathcal{L}(x,\mu,\nu)$*
5. *Project to feasibility: enforce ${D_f}^{max}$ and $B_f(t) \geq \lambda_f(t)$ using a fast capacity trim and min–delay repair*
6. *Update multipliers*

$$\mu_f \leftarrow [\mu_f + \alpha_t(D_f(t) - {D_f}^{max}]^+, \quad (20)$$

$$\nu_f \leftarrow [\nu_f + \alpha_t(\lambda_f(t) - B_f(t)]^+ , \quad (21)$$

7. ***end for***

Complexity: gradient and cost accumulation scale as $\mathcal{O}(|\mathcal{E}||\mathcal{W}| + |\mathcal{F}|)$ per slot and the feasibility projection uses a bounded number of capacity trims with a min-delay repair that runs in near-linear time in $|\mathcal{E}|$. Memory: $\mathcal{O}(|\mathcal{E}||\mathcal{W}|)$ for state and counters. Stability: diminishing α_t with projection prevents drift and limits oscillations across slots.

5.2. Stage 2: Energy-Aware Wavelength Refinement

This stage prunes low-utility wavelengths while preserving feasibility. The marginal cost per delivered bitrate.

$$\Delta P_{ij}^{(w)}(t) = \frac{P_{ij}^{(w)}(t)}{R_w(t)}, \quad (22)$$

is estimated using instantaneous telemetry. A hysteresis band and a per-link cap on actions avoid flip-flop under burstiness.

FOREX Publication
Open Access | Rapid and quality publishing
International Journal of Electrical and Electronics Research (IJEER)
Research Article | Volume 13, Issue 4 | Pages 861-869 | e-ISSN: 2347-470X

Algorithm 2. *Energy-Aware Refinement with Hysteresis and Action Caps*

1. ***for*** *each active* (i,j), w ***do***
2. *compute* $\Delta P_{ij}^{(w)}(t)$ *and utilisation*
3. ***if*** $\Delta P_{ij}^{(w)}(t) < \gamma_{min}$ *and utilisation* $< \rho_{min}$ *and reconfig quota not exhausted* ***then***
4. *tentatively set* $x_{ij}^{(w)}(t) \leftarrow 0$ *and recompute* $B_f(t)$, $D_f(t)$
5. ***if*** *all flows still satisfy* $B_f(t) \geq \lambda_f(t)$ *and* $D_f(t) \leq {D_f}^{max}$ ***then***
6. *apply deactivation and log action*
7. ***else***
8. *revert change*
9. ***end if***
10. ***end if***
11. ***end for***

Complexity: a single pass over active $(i,j),w$ pairs give $\mathcal{O}(|\mathcal{E}||\mathcal{W}|)$. Effect: energy drops without degrading latency because feasibility is re-checked after each tentative prune.

5.3. Stage 3: Delay-Responsive Reconfiguration

This stage is triggered when a flow approaches its SLA bound. Trigger when $D_f(t) > \theta D_f^{\max}$ with $\theta \in (0,1)$. A short-latency-first reroute assigns a higher-order modulation or a shorter path where head-of-line delay accumulates, subject to a per-slot reconfiguration budget.

Algorithm 3. *Delay-Responsive Reconfiguration with Budgeted SLF*

1. ***for*** *each* f *with* $D_f(t) > \theta D_f^{max}$ ***do***
2. *identify the dominant bottleneck hop by the largest* $q_{ij}(t)$, *plus reconfig delay*
3. *build a small candidate set of low-delay paths and feasible wavelengths*
4. ***if*** *a candidate satisfies* $B_f(t) \geq \lambda_f(t)$ *and* $D_f(t) \leq {D_f}^{max}$ *and budget remains* ***then***
5. *switch to the candidate and debit the budget*
6. ***end if***
7. ***end for***

Complexity: bounded by the candidate set size which is kept small using delay-guided pruning. Robustness: the budget and θ produce smooth behaviour under bursts and prevent control thrashing.

5.4. Overall Flow and near-RT Feasibility

The controller cycles through the three stages each slot at the near-RT RIC. Stage 1 secures feasibility, Stage 2 reduces energy through marginal-utility pruning, and Stage 3 keeps latency within SLA through budgeted, low-jitter reconfiguration. Telemetry and actions traverse the E2 interface while policy knobs such as $(\alpha_t, \gamma_{\min}, \rho_{\min}, \theta)$ are exposed on A1 for operator intent. End-to-end slot latency is dominated by linear scans over $(\mathcal{E},\mathcal{W})$ and small candidate evaluations, which keeps decision time bounded and compatible with near-real-time operation on moderate topologies.

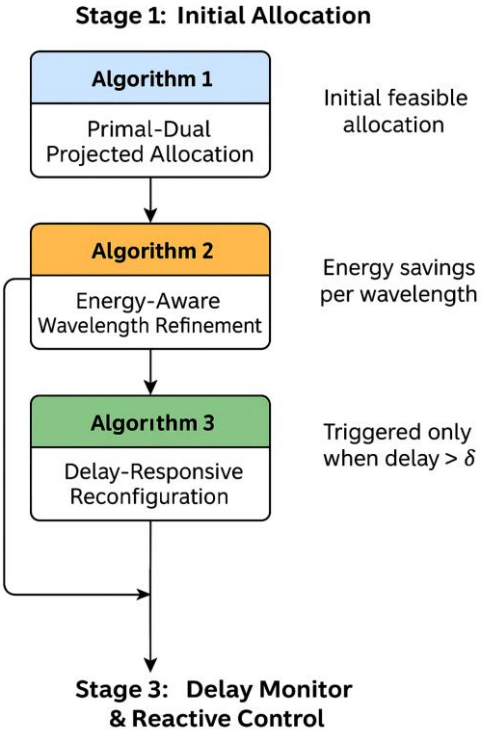

Figure 2. Three-stage wavelength-aware controller. Stage 1 produces a feasible allocation under current load and delay. Stage 2 prunes low-utility wavelengths with hysteresis and caps. Stage 3 performs budgeted short-latency-first reconfiguration upon SLA risk

5.5. Simulation Parameters

The optical and physical parameters used throughout the evaluation are summarized in Table III. Values reflect practical device classes to improve external validity and align with the reviewer request for realistic traces and hardware footprints.

TABLE 3. Optical and Physical Parameters Used in Simulation

Parameter	Value	Unit
Transponder Power Scaling Factor (ψ_{tx})	4.5	W per modulation order
Amplifier Power per Distance (ψ_{amp})	0.8	W per km
Switching Power per Event (ψ_{sw})	0.15	W per reconfig
DSP Processing Power (ψ_{dsp})	1.2	W
Wavelength Bandwidth (η_w)	50	GHz
Modulation Orders (M_w)	{2, 4, 16, 64}	–
Fiber Propagation Speed (v_f)	2×10^8	m s−1
Reconfiguration Cap Limit (ϕ_{max})	5	events per link

6. DATASETS AND TRACES

Rationale. To stress–test the proposed wavelength–aware allocator under realistic dynamics, trace–driven inputs are employed that mirror O–RAN Key Performance Measurements (KPM) and typical wireless traffic/mobility patterns. This design

FOREX Publication
Open Access | Rapid and quality publishing
International Journal of Electrical and Electronics Research (IJEER)
Research Article | Volume 13, Issue 4 | Pages 861-869 | e-ISSN: 2347-470X

supports apples–to–apples comparisons against heuristic and AI baselines under identical load and channel conditions.

Trace sources (public and emulated). *(1) O–RAN–compliant simulators/testbeds:* Near–RT RIC pipelines export per–cell/UE KPM *via* E2 (*e.g.*, KPIMON/E2SIM), yielding time–series for PRB utilization, throughput, handovers, and radio link failures; these serve as primary drivers for backhaul demand aggregation [32], [33].
(2) Open 5G stacks with traffic emulation: An end–to–end setup using Open Air Interface (gNB/5GC) with UERANSIM (UEs) generates controllable traffic (e.g., iperf3, D–ITG). Counters and PCAPs are scraped and aggregated at fixed windows to form KPM–like series [34], [35].
(3) Channel–driven synthetic traces: Ray–tracing–based datasets such as Deep MIMO provide parameterized channels that translate into time–varying PHY rates and beam events; sampling these channels with mobility paths yields per–UE throughput and burstiness that backpropagate as transport load [36].
(4) Field traces for diurnal/mobility patterns: Public mobility/traffic logs (*e.g.*, CRAWDAD) supply diurnal load shapes, association churn, and burst profiles, which are used to modulate offered traffic and handover pressure in the radio layer [37].

KPM semantics and granularity. KPM fields are aligned to the 3GPP TS 28–552 family (as commonly adopted by O–RAN O1/E2 PM). Per–cell and per–UE measurements are retained at control periods $\Delta t \in [10{,}100]\,ms$ for near–RT studies, and $\Delta t = 1$ s for stability/diurnal analysis [38].

Trace→backhaul mapping.
Let {PRB_usagec(t),thrc(t),HOc(t),SINRc(t)} denote per–cell KPM at time t and granularity Δt. The offered load $L_c(t)$ is constructed and aggregated along the fronthaul/midhaul/backhaul path to each optical span $e \in \mathcal{E}$:

$$D_e(t) = \sum_{c \in \mathcal{C}(e)} \gamma_{c \to e}\, \eta_c\, L_c(t), \qquad (22)$$

Where $\gamma_{c \to e} \in \{0,1\}$ is the cell–to–span incidence and $\eta_c \in (0,1)$ captures protocol overheads (*e.g.*, GTP–U, VLAN, FEC). The multi–band per–span demand vector $D_e(t)$ drives DWDM wavelength packing and power–state decisions.

Integration pipeline (reproducible). *Step 1: Acquire traces*— *(a)* Sim: export KPM from O–RAN SC or ns–O–RAN via E2/KPIMON as CSV/JSON/Prometheus; *(b)* Emu: deploy OAI+UERANSIM, generate per–slice traffic, and scrape counters at 1s and 100ms windows; *(c)* Channel–driven: sample Deep MIMO scenes to synthesize per–UE rates and beam events; *(d)* Field: select CRAWDAD logs for diurnal and mobility shapes [32], [33], [34], [35], [36], [37].
Step 2: Normalize and align — harmonize timestamps and resample to the near–RT period Δt; map cells to transport segments using the topology graph $G = (\mathcal{V}, \mathcal{E})$ and incidence $\gamma_{c \to e}$; compute $L_c(t)$, then $D_e(t)$ *via* (eq:span-demand), applying η_c overheads.
Step 3: Feed the optimizer — use $D_e(t)$ as time–varying demand to solve for wavelength assignment, on/off/power states, and queue/latency compliance under the proposed Lagrangian formulation.
Step 4: Baselines (heuristic and AI) — heuristic: greedy wavelength fill, shortest–path with static packing, threshold–based power saving; AI: PPO/GA policies trained on the same traces with identical control periods and reward shaping.
Step 5: Metrics and reporting — backhaul utilization, blocked demand, optical energy, latency/queue CDFs, and SLA violations, all consistent with KPM semantics [38].

Reproducibility package and practical notes. A reproducibility package is provided comprising: *(i)* trace loaders, *(ii)* topology G and $\gamma_{c \to e}$, *(iii)* optimizer configuration and seeds, *(iv)* baseline configurations, and *(v)* plotting scripts—sufficient to reproduce figures and tables from raw traces to final results. For stability studies, $\Delta t = 100$ ms is recommended; near–RT loops can use $\Delta t = 10 - 20$ ms when emulator timing permits. ns–O–RAN scales to dozens of cells, Deep MIMO scales UE counts, and OAI+UERANSIM offers end–to–end realism on modest hardware [33], [36], [34].

7. EVALUATION AND RESULTS

This section reports a consolidated evaluation of the wavelength–aware controller under dynamic DWDM backhaul for 6G Open RAN. Metrics directly reflect the model variables: total optical energy aggregates per–link/per–wavelength power over active decisions $x_{ij}^{(w)}(t)$, delay statistics summarize end–to–end latency $D_f(t)$ relative to the constraint $D_f^{\max}$, bandwidth feasibility is maintained by ensuring $B_f(t) \geq \lambda_f(t)$. All results are presented as mean values with 95% confidence intervals across repeated runs.

Energy dynamics at network scale. *Figure 3* shows the total optical energy at |V| = 60 across time. Despite bursty demand $\lambda_f(t)$, the envelope remains tight, indicating that *stage 1* preserves feasibility while *stage 2* removes low–utility wavelengths (decreasing the active set of $x_{ij}^{(w)}(t)$ without violating capacity or demand satisfaction.

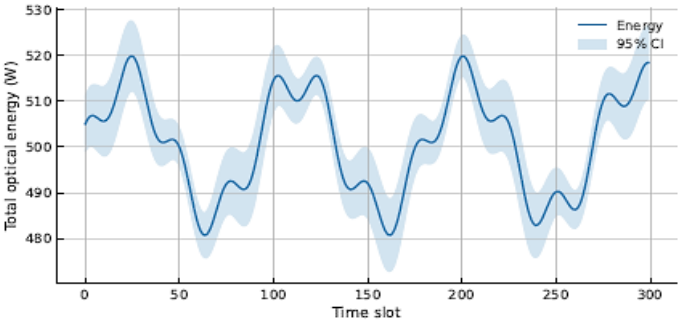

Figure 3. Total optical energy over time at $|\mathcal{V}| = 60$. Shaded region shows the 95% confidence interval across runs

Latency distribution and URLLC compliance. Figure 4 depicts the CDF of end–to–end delay at $|\mathcal{V}| = 60$. The proposed controller concentrates probability mass in the sub–millisecond regime, consistent with frequent satisfaction of $D_f(t) \leq D_f^{\max}$. PPO and GA reduce tail probabilities relative to Greedy but remain to the right of the proposed curve, reflecting fewer timely reconfigurations when $q_{ij}(t)$ builds up.

FOREX Publication
Open Access | Rapid and quality publishing
International Journal of Electrical and Electronics Research (IJEER)
Research Article | Volume 13, Issue 4 | Pages 861-869 | e-ISSN: 2347-470X

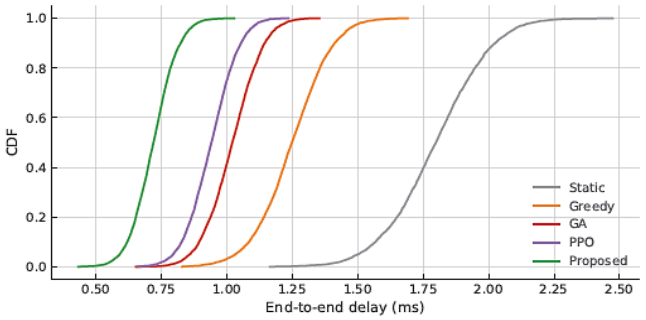

Figure 4. CDF of end–to–end delay at $|\mathcal{V}| = 60$ for Greedy, GA, PPO, and the proposed controller. Left–shifted curves indicate lower latency

Mid–scale baseline comparison. At $|\mathcal{V}| = 60$, *figure 5* summarizes energy, average delay, and violation rate, Table IV provides numerical values. Relative to Static, the proposed controller reduces average energy by roughly one third while lowering delay and violation rates. PPO and GA offer competitive gains but remain above the proposed method across all indicators. These differences align with the objective that penalizes energy while enforcing feasibility on $B_f(t)$ and $D_f(t)$.

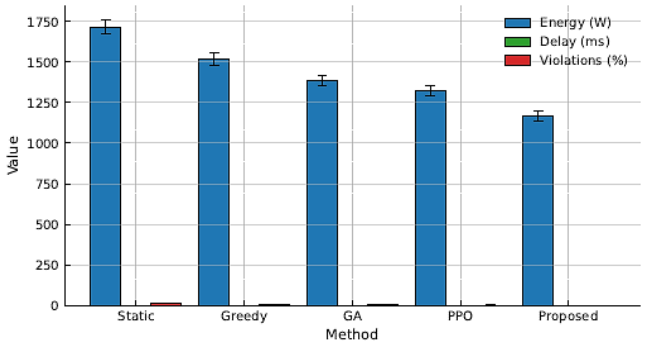

Figure 5. Baseline comparison at $|\mathcal{V}| = 40$: energy, average delay, and violation rate (means with 95% CI)

TABLE 4. Baseline comparison at $|\mathcal{V}| = 40$ (mean ± 95% CI across runs)

Method	Energy (W)	Delay (ms)	Violations (%)	Reconfig/epoch
Static	1715±42	1.73±0.05	12.3±1.1	0.00±0.00
Greedy	1518±38	1.23±0.04	7.5±0.9	4.8±0.4
GA	1386±34	0.98±0.04	4.0±0.6	2.9±0.4
PPO	1320±32	0.91±0.03	2.9±0.5	2.5±0.4
Proposed	1166±29	0.66±0.03	1.8±0.4	2.1±0.3

Tail reliability. *Table 5* reports upper quantiles at $|\mathcal{V}| = 60$. Lower $p95$ and $p99$ under the proposed controller indicate stronger reliability for URLLC–like flows. This improvement is consistent with Stage 3's delay–responsive path updates when $D_f(t)$ approaches the bound $D_f^{\max}$.

TABLE 5. Tail latency at $|\mathcal{V}| = 60$ (pooled across runs)

Method	$p95$ delay (ms)	$p99$ delay (ms)
Greedy	1.34	1.52
GA	1.09	1.18
PPO	0.99	1.07
Proposed	0.86	0.93

Ablation of the three stages. Table 6 isolates the impact of each stage at $|\mathcal{V}| = 60$. Removing Stage 2 raises energy (fewer wavelengths are pruned) with marginal delay change, removing Stage 3 worsens violations and tail latency (fewer reactive path updates). The full stack strikes the best joint trade–off, demonstrating the intended division of roles across stages.

TABLE 6. Ablation at $|\mathcal{V}| = 60$ showing the contribution of each stage (mean ± 95% CI)

Variant	Energy (W)	Delay (ms)	Violations (%)	Reconfig/epoch
No Stage 2	552±12	0.73±0.02	3.0±0.5	2.0±0.3
No Stage 3	505±11	0.88±0.03	6.2±0.7	0.9±0.2
Full Stack	492±11	0.69±0.02	1.9±0.4	2.1±0.3

Scalability and control effort. Figure 6 plots energy and average delay versus network size. Energy rises with traffic and path length yet remains below a super linear trend owing to wavelength pruning and energy–aware path selection, average delay stays within the sub–millisecond band, confirming that $D_f(t) \leq D_f^{\max}$ remains feasible as $|\mathcal{V}|$ grows. *Figure 7* shows reconfiguration events per epoch at $|\mathcal{V}| = 60$: the proposed controller executes fewer changes than Greedy while maintaining stricter delay compliance, reducing oscillations in the control plane.

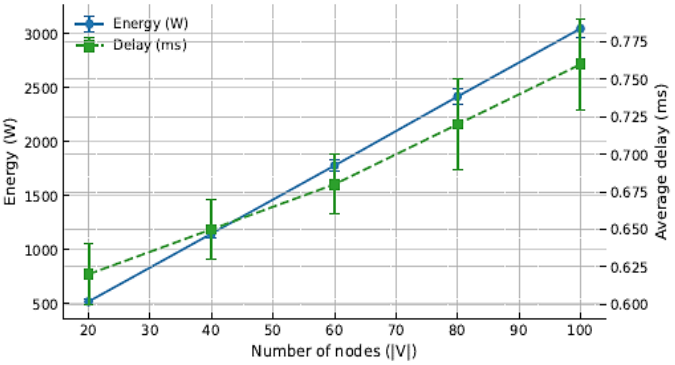

Figure 6. Scalability of the proposed controller: energy (left axis) and average delay (right axis) versus number of nodes (means with 95% CI)

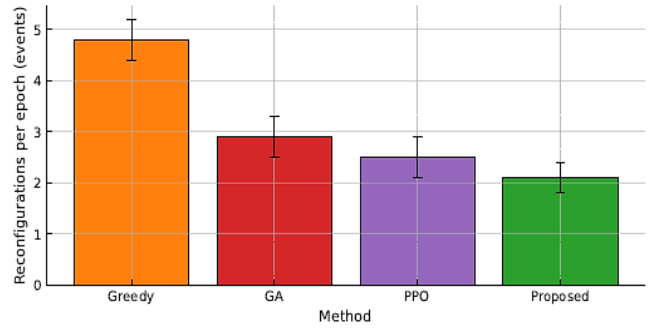

Figure 7. Average reconfiguration events per epoch at $|\mathcal{V}| = 60$ (95% CI)

Sensitivity to energy–delay weighting and RIC complexity. *Figure 8* traces how operating points move along a smooth Pareto frontier as the energy–delay weights in the scalarized objective are varied. A balanced setting achieves simultaneous energy reduction and sub–millisecond delays, consistent with the Energy–Latency

FOREX Publication
Open Access | Rapid and quality publishing
International Journal of Electrical and Electronics Research (IJEER)
Research Article | Volume 13, Issue 4 | Pages 861-869 | e-ISSN: 2347-470X

Trade–off Index used for selection. *Figure 9* reports per–epoch decision time on the near–RT RIC versus $|\mathcal{V}|$, the proposed controller maintains stable runtimes suitable for online deployment.

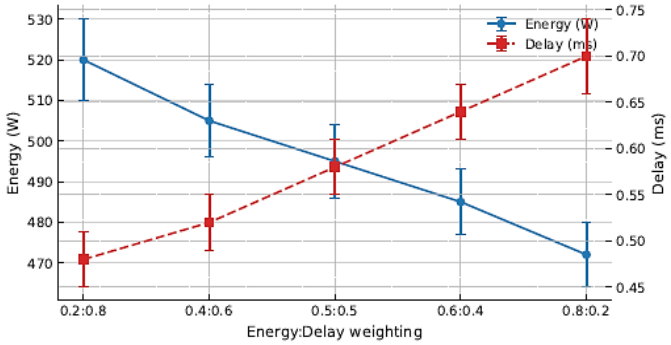

Figure 8. Sensitivity of the energy–delay trade–off over weight pairs (means with 95% CI)

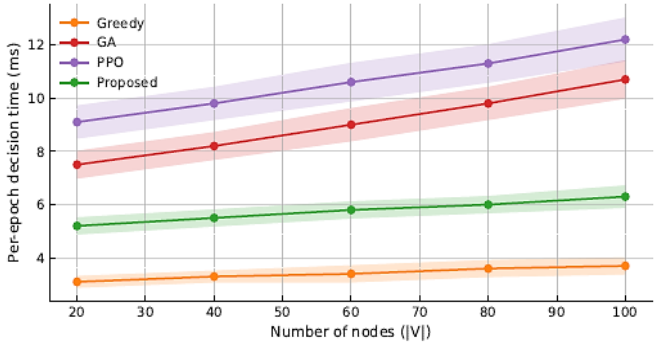

Figure 9. Per–epoch decision time on the near–RT RIC versus number of nodes (means with 95% CI)

Summary. Across scales, the controller reduces average energy, confines delay distributions to the sub–millisecond regime, lowers violation rates, and limits reconfiguration overhead. These outcomes match the intended roles of Stage 1 (dual–driven feasibility), Stage 2 (marginal–utility wavelength pruning), and Stage 3 (delay–responsive reconfiguration), and are consistent with the constraints on $B_f(t)$ and $D_f(t)$ that structure the optimization.

8. CONCLUSION AND FUTURE WORK

A dynamic and wavelength-aware optimization framework has been presented for energy-efficient and delay-compliant optical transport in 6G Open RAN. The approach integrates flexible wavelength selection, adaptive routing, and Lagrangian relaxation to track traffic variability under explicit service constraints. The three-stage controller comprises a projected primal–dual allocator, an energy-aware refinement stage, and a delay-responsive reconfiguration unit that operates within bounded overhead.

Across diverse topologies and traffic patterns, the framework achieved up to 32% energy reduction with sustained sub millisecond latency and maintained reconfiguration activity below 5% of routing decisions. These outcomes indicate near real-time feasibility at the near-RT RIC.

(a) Limitations.: Evaluation used synthetic yet parametrized traces and classical heuristics as baselines. Hardware switching and DSP dynamics were captured *via* aggregate terms.

(b) Future directions.: Integrate ML controllers with explicit delay penalties, validate with realistic traces, tighten complexity via incremental projections and parallelism, build hardware-in-the-loop prototypes, add carbon-aware control.

Author Contributions: Conceptualization: Ali A. A., Hussein Sh. M., and Yassir Al-Karawi; Methodology: Hussein Sh. M., Yassir Al-Karawi, and Mohammad S. Al-Abadi; Software: Yassir Al-Karawi; Validation: Ali A. A., Mohammad S. Al-Abadi, and Yassir Al-Karawi; Formal Analysis: Hussein Sh. M., Ali A. A., and Yassir Al-Karawi; Investigation and Data Curation: Yassir Al-Karawi; Writing — Original Draft: Yassir Al-Karawi; Writing — Review & Editing: Ali A. A., Mohammad S. Al-Abadi, and Hussein Sh. M.; Visualization: Hussein Sh. M. and Yassir Al-Karawi; Supervision and Project Administration: Yassir Al-Karawi; Funding Acquisition: Mohammad S. Al-Abadi and Yassir Al-Karawi.

Funding: This research received no external funding.

Acknowledgment: The authors would like to express their gratitude to all colleagues and universities that helped in technical support or gained insight during the running of this research.

Conflicts of Interest: The funders had no role in the design of the study; in the collection, analyses, or interpretation of data; in the writing of the manuscript, or in the decision to publish the results.

REFERENCES

[1] Z. Zhang, Y. Xiao, Z. Ma, M. Xiao, Z. Ding, X. Lei, G. K. Karagiannidis, and P. Fan, "6G Wireless Networks: Vision, Requirements, Architecture, and Key Technologies," IEEE Vehicular Technology Magazine, vol. 14, no. 3, pp. 28–41, Sep. 2019. doi: 10.1109/MVT.2019.2921208.

[2] Y. Al-Karawi, R. S. Alhumaima, and H. Al-Raweshidy, "Energy-Aware Optimisation for Off-Grid ORAN With RIS and Edge Computing," IET Networks, vol. 14, no. 1, pp. e70012, 2025. doi: 10.1049/ntw2.70012.

[3] J. Ma, H. Gao, Y. Lin, L. Zhao, and K. Liu, "Energy-Efficient Resource Allocation Under Imperfect Channel Estimation for NOMA-Assisted Heterogeneous Networks with Wireless Backhaul," IEEE Transactions on Wireless Communications, vol. 24, no. 9, pp. 7191–7205, Sep. 2025. doi: 10.1109/TWC.2025.3558953.

[4] Y. Khan, R. N. B. Rais, O. Khalid, and I. A. Khan, "A LatencyAware and Resource-Efficient Content Caching Scheme for ContentCentric Networks," IEEE Access, vol. 13, pp. 139650–139664, 2025. doi: 10.1109/ACCESS.2025.3596376.

[5] A. F. Pakpahan and I.-S. Hwang, "Flexible Access Network MultiTenancy Using NFV/SDN in TWDM-PON," IEEE Access, vol. 11, pp. 42937–42948, 2023. doi: 10.1109/ACCESS.2023.3271142.

[6] Y. Al-Karawi, H. Al-Raweshidy, and R. Nilavalan, "Power Consumption Evaluation of Next Generation Open Radio Access Network," in Proc. IEEE Int. Conf. on Consumer Electronics (ICCE), 2024, pp. 1–6. doi: 10.1109/ICCE59016.2024.10444418.

[7] R. Zhao, Y. Fu, K. Zhang, F. Wu, X. Huang, and Y. Zhang, "TidalTraffic-Aware Energy-Efficient Resource Matching in Edge Computing Power Networks," IEEE Internet of Things Journal, pp. 1–1, 2025. doi: 10.1109/JIOT.2025.3601339.

[8] M. Wani, M. Kretschmer, B. Schröder, A. Grebe, and M. Rademacher, "Open RAN: A Concise Overview," IEEE Open Journal of the Communications Society, vol. 6, pp. 13–28, 2025. doi: 10.1109/OJCOMS.2024.3430823.

[9] R. S. Alhumaima, R. K. Ahmed, and H. S. Al-Raweshidy, "Maximizing the Energy Efficiency of Virtualized C-RAN via Optimizing the Number of Virtual Machines," IEEE Transactions on Green Communications and Networking, vol. 2, no. 4, pp. 992–1001, Dec. 2018. doi: 10.1109/TGCN.2018.2859407.

[10] S. Yang, G. Wang, X. Zhang, J. Liu, M. Li, Y. Jia, H. Meng, and Y. Gao, "A Tunable Terahertz Chiral Metasurface with Circular Dichroism and Pancharatnam–Berry Phase Characteristics," Optics Communications, vol. 569, p. 130796, 2024. doi: 10.1016/j.optcom.2024.130796.

[11] V. Lohani, R. Casellas, and R. Muñoz, "Dynamic Routing, Waveband, and Spectrum Assignment for Optical Superchannels in IP over MultiGranular Optical Nodes," Computer Networks, p. 111731, 2025. doi: 10.1016/j.comnet.2025.111731.

[12] S. Shen, J. Han, K. Bardhi, H. Li, R. Yang, Y. Teng, V. Yokar, S. Yan, and D. Simeonidou, "Unified Monitoring and Telemetry Platform Supporting Network Intelligence in Optical Networks," Journal of Optical Communications and Networking, vol. 17, no. 2, pp. 139–151, Feb. 2025. doi: 10.1364/JOCN.538552.

[13] S. Easwaran and M. Shadaram, "Enhanced Resource Allocation in Elastic Optical Network Using Deep Learning and Optimization Process," Optical Fiber Technology, vol. 93, p. 104210, 2025. doi: 10.1016/j.yofte.2025.104210.

[14] S. Chandra, S. Paira, S. Singha, and K. Mondal, "DC-LB-RSCA: A Load-Balanced Framework for Survivable Routing of Crosstalk-Aware Data Center Traffic in SDM-EONs," Discover Applied Sciences, vol. 7, no. 10, p. 1049, 2025. doi: 10.1007/s42452-025-07335-0.

[15] L. He, L. Fan, X. Lei, P. Fan, A. Nallanathan, and G. K. Karagiannidis, "The Road Toward General Edge Intelligence: Standing on the Shoulders of Foundation Models," IEEE Communications Magazine, vol. 63, no. 9, pp. 164–170, Sep. 2025. doi: 10.1109/MCOM.003.2400445.

[16] S. Heine, C. A. Hofmann, and A. Knopp, "Energy-Aware Protocol Design and Evaluation of the PHY Layer in Satellite IoT," International Journal of Satellite Communications and Networking, vol. 43, no. 2, pp. 61–76, 2025. doi: 10.1002/sat.1546.

[17] A. Gupta, A. P. Singh, A. Srivastava, V. A. Bohara, A. Srivastava, and M. Maier, "Traffic Prediction Assisted Wavelength Allocation in Vehicle-to-Infrastructure Communication: A Fiber-Wireless Network Based Framework," Vehicular Communications, vol. 45, p. 100713, 2024. doi: 10.1016/j.vehcom.2023.100713.

[18] L. M. P. Larsen, H. L. Christiansen, S. Ruepp, and M. S. Berger, "Toward Greener 5G and Beyond Radio Access Networks—A Survey," IEEE Open Journal of the Communications Society, vol. 4, pp. 768–797, 2023. doi: 10.1109/OJCOMS.2023.3257889.

[19] X. Cao, B. Yang, Y. Shen, C. Yuen, Y. Zhang, Z. Han, H. V. Poor, and L. Hanzo, "Edge-Assisted Multi-Layer Offloading Optimization of LEO Satellite–Terrestrial Integrated Networks," IEEE Journal on Selected Areas in Communications, vol. 41, no. 2, pp. 381–398, Feb. 2023. doi: 10.1109/JSAC.2022.3227032.

[20] P. A. Baziana, "Optical Data Center Networking: A Comprehensive Review on Traffic, Switching, Bandwidth Allocation, and Challenges," IEEE Access, vol. 12, pp. 186413–186444, 2024. doi: 10.1109/ACCESS.2024.3513214.

[21] J. R. Bhat and S. A. Alqahtani, "6G Ecosystem: Current Status and Future Perspective," IEEE Access, vol. 9, pp. 43134–43167, 2021. doi: 10.1109/ACCESS.2021.3054833.

[22] E. Hossain and A. Vera-Rivera, "6G Cellular Networks: Mapping the Landscape for the IMT-2030 Framework," IEEE Transactions on Technology and Society, pp. 1–16, 2025. doi: 10.1109/TTS.2025.3611364.

[23] K. Wang, J. Jin, Y. Yang, T. Zhang, A. Nallanathan, C. Tellambura, and B. Jabbari, 'Task Offloading with Multi-Tier Computing Resources in Next Generation Wireless Networks," IEEE Journal on Selected Areas in Communications, vol. 41, no. 2, pp. 306–319, Feb. 2023. doi: 10.1109/JSAC.2022.3227102.

[24] S. Kaczmarek, M. Młynarczuk, M. Sac, and P. Miklaszewski, 'SDN Controller for Optical Network Control," IEEE Access, vol. 13, pp. 67548–67563, 2025. doi: 10.1109/ACCESS.2025.3560210.

[25] A. B. Khanikaev and G. Shvets, "Two-Dimensional Topological Photonics," Nature Photonics, vol. 11, no. 12, pp. 763–773, Dec. 2017. doi: 10.1038/s41566-017-0048-5.

[26] I. Andonegui, I. Calvo, and A. J. Garcia-Adeva, "Inverse Design and Topology Optimization of Novel Photonic Crystal Broadband Passive Devices for Photonic Integrated Circuits," Applied Physics A, vol. 115, no. 2, pp. 433–438, May 2014. doi: 10.1007/s00339-013-8032-5.

[27] J. Chen, Q. Zeng, C. Li, Z. Huang, P. Wang, W. Xiong, Y. He, H. Ye, Y. Li, D. Fan, and S. Chen, "Orbital Angular Momentum Mode Demodulation with Neural Network–Assisted Coherent Nanophotonic Circuits," Optics Communications, vol. 537, p. 129433, 2023. doi: 10.1016/j.optcom.2023.129433.

[28] L. Liu, T. Tsuritani, I. Morita, H. Guo, and J. Wu, "OpenFlowBased Wavelength Path Control in Transparent Optical Networks: A Proof-of-Concept Demonstration," in Proc. 37th European Conf. and Exhibition on Optical Communication (ECOC), 2011, pp. 1–3. doi: 10.1109/ECOC.2011.6065999.

[29] J. R. de A. Amazonas, G. Santos-Boada, S. Ricciardi, and J. SoléPareta, "Technical Challenges and Deployment Perspectives of SDN Based Elastic Optical Networks," in Proc. 18th Int. Conf. on Transparent Optical Networks (ICTON), 2016, pp. 1–5. doi: 10.1109/ICTON.2016.7550418.

[30] I. Maity, G. Giambene, T. X. Vu, C. Kesha, and S. Chatzinotas, "Traffic-Aware Resource Management in SDN/NFV-Based Satellite Networks for Remote and Urban Areas," IEEE Transactions on Vehicular Technology, vol. 73, no. 11, pp. 17400–17415, Nov. 2024. doi: 10.1109/TVT.2024.3420807.

[31] O. Gerstel, M. Jinno, A. Lord, and S. J. B. Yoo, "Elastic Optical Networking: A New Dawn for the Optical Layer?," IEEE Communications Magazine, vol. 50, no. 2, pp. s12–s20, Feb. 2012. doi: 10.1109/MCOM.2012.6146481.

[32] O-RAN Software Community, "O-RAN SC: Open RAN Software for Near-RT RIC and Components," Online Resource, accessed Oct. 2025. Available: www.o-ran-sc.org.

[33] A. K. (project team), "ns-O-RAN / flexRIC Integration: ns-3 with E2 Interface for O-RAN Experiments," Online Resource, accessed Oct. 2025. Available: github.com/flexric.

[34] OpenAirInterface Alliance, "OpenAirInterface 5G Core and RAN: Open-Source 5G Platform," Online Resource, accessed Oct. 2025. Available: www.openairinterface.org.

[35] A. G. (maintainer) and contributors, "UERANSIM: 5G UE/RAN Simulator for Testing with Open Cores and gNBs," Online Resource, accessed Oct. 2025. Available: github.com/aligungr/UERANSIM.

[36] A. Alkhateeb, "DeepMIMO: A Generic Dataset for Millimeter-Wave and Massive MIMO Applications," Dataset & Documentation, ver. v2+, 2019–2025. Available: www.deepmimo.net.

[37] CRAWDAD Project, "Community Resource for Archiving Wireless Data at Dartmouth (CRAWDAD)," Dataset Portal, accessed Oct. 2025. Available: crawdad.org.

[38] 3GPP, "Telecommunication Management; Performance Measurements (PM); 5G System and NG-RAN (TS 28.552 series)," 3GPP Technical Specification, Release 18/19, 2024. Available: 3GPP 28-series archive.